Meiotic Consequences of Genetic Divergence Across the Murine Pseudoautosomal Region

Beth L. Dumont[1]
Department of Biological Sciences, Initiative in Biological Complexity, North Carolina State University, Raleigh, North Carolina 27695
ORCID ID: 0000-0003-0918-0389 (B.L.D.)

ABSTRACT The production of haploid gametes during meiosis is dependent on the homology-driven processes of pairing, synapsis, and recombination. On the mammalian heterogametic sex chromosomes, these key meiotic activities are confined to the pseudoautosomal region (PAR), a short region of near-perfect sequence homology between the *X* and *Y* chromosomes. Despite its established importance for meiosis, the PAR is rapidly evolving, raising the question of how proper *X*/*Y* segregation is buffered against the accumulation of homology-disrupting mutations. Here, I investigate the interplay of PAR evolution and function in two interfertile house mouse subspecies characterized by structurally divergent PARs, *Mus musculus domesticus* and *M. m. castaneus*. Using cytogenetic methods to visualize the sex chromosomes at meiosis, I show that intersubspecific F_1 hybrids harbor an increased frequency of pachytene spermatocytes with unsynapsed sex chromosomes. This high rate of asynapsis is due, in part, to the premature release of synaptic associations prior to completion of prophase I. Further, I show that when sex chromosomes do synapse in intersubspecific hybrids, recombination is reduced across the paired region. Together, these meiotic defects afflict ~50% of spermatocytes from F_1 hybrids and lead to increased apoptosis in meiotically dividing cells. Despite flagrant disruption of the meiotic program, a subset of spermatocytes complete meiosis and intersubspecific F_1 males remain fertile. These findings cast light on the meiotic constraints that shape sex chromosome evolution and offer initial clues to resolve the paradox raised by the rapid evolution of this functionally significant locus.

KEYWORDS pseudoautosomal region; aneuploidy; recombination; meiosis; *Mus musculus*

THE processes of meiotic pairing, synapsis, and recombination are essential for progression through the first meiotic division and the formation of haploid gametes. Unpaired, asynapsed chromatin is transcriptionally silenced (Shiu *et al.* 2001; Baarends *et al.* 2005), and the aberrant repression of key genes regulating meiotic progression can cause premature arrest of the meiotic cell cycle (Turner *et al.* 2005; Burgoyne *et al.* 2009). A minimum of one crossover per bivalent is needed to ensure its stable orientation at the metaphase plate (Mather 1938; Nicklas 1974), and homologous chromosome pairs that lack an obligate crossover are susceptible to nondisjunction at the first meiotic division (Hawley *et al.* 1994; Lamb *et al.* 1996; Ross *et al.* 1996). As a consequence, meiotic pairing, synapsis, and recombination defects are directly linked to infertility and chromosome aneuploidy (Hassold and Hunt 2001; Cohen *et al.* 2006; Burgoyne *et al.* 2009; Handel and Schimenti 2010), outcomes with severe consequences for organismal fitness.

The mammalian sex chromosomes present a notable deviation to these general rules of meiosis. Although the *X* and *Y* are derived from an ancestral pair of homologous autosomes, the long-term suppression of recombination between them has eroded sequence homology across most of their length (Graves *et al.* 1995; Charlesworth 1996; Lahn and Page 1999). In most mammals, the only vestige of this ancestral identity is a short region of terminal homology known as the pseudoautosomal region (PAR). The key homology-driven steps of meiotic pairing and recombination are confined to this narrow zone of residual sequence identity (Burgoyne 1982; Mangs and Morris 2007), rendering the PAR one of the most functionally important regions of the genome. Failure to

doi: 10.1534/genetics.116.189092
Manuscript received March 10, 2016; accepted for publication January 3, 2017; published Early Online January 18, 2017.
Available freely online through the author-supported open access option.
Supplemental material is available online at www.genetics.org/lookup/suppl/doi:10.1534/genetics.116.189092/-/DC1.
[1]Corresponding author: The Jackson Laboratory, North Carolina State University, 600 Main St., Bar Harbor, ME 04609. E-mail: beth.dumont@jax.org

initiate or maintain pairing across the PAR is associated with meiotic arrest (Matsuda *et al.* 1982, 1992) and reduced recombination across this region has been directly linked to sex chromosome nondisjunction in humans (Hassold *et al.* 1991; Shi *et al.* 2001). Expectedly, mutations that disrupt sequence homology across the PAR or interfere with sex chromosome pairing are often associated with male infertility and elevated rates of sex chromosome aneuploidy (Gabriel-Robez *et al.* 1990; Matsuda *et al.* 1992; Mohandas *et al.* 1992; Korobova *et al.* 1998; Burgoyne and Evans 2000; Jorgez *et al.* 2011).

Despite its central role in mammalian meiosis, the PAR is rapidly evolving, both at the level of DNA sequence and structure (Kipling *et al.* 1996; Perry and Ashworth 1999; Schiebel *et al.* 2000; Filatov and Gerrard 2003; Bussell *et al.* 2006; White *et al.* 2012a). A comparative sequence analysis of human-orangutan orthologs found that noncoding divergence in PAR-linked genes is more than twice the rate of evolution at autosomal genes (Filatov and Gerrard 2003). Similarly, the rate of nucleotide substitution across the mouse PAR is several-fold higher than that for adjacent *X*-linked regions (Perry and Ashworth 1999; White *et al.* 2012a). PAR-length polymorphisms have been characterized in both human and mouse (Kipling *et al.* 1996; White *et al.* 2012a; Mensah *et al.* 2014), and there is rapid structural rearrangement of the PAR in closely related vole species (Acosta *et al.* 2011; Borodin *et al.* 2012). Owing to challenges associated with genotyping and sequencing this region of the genome, the full extent of natural genetic variation in the mammalian PAR is still in an active discovery phase (Mensah *et al.* 2014).

Together, the PAR's essential meiotic roles and dramatic evolutionary trends present an intriguing biological conundrum: How does such a functionally significant region of the genome—and, notably, one whose function is directly dependent upon the preservation of homology between two chromosomes—evolve so rapidly? Answers to this question could provide important new insights into the general requirements for sequence homology and pairing at meiosis, as well as clues into the selective forces that constrain the evolution of sex chromosomes.

Toward this goal, one potentially informative experimental approach is to directly assess the meiotic consequences of PAR divergence in hybrids characterized by distinct *X*- and *Y*-linked PAR sequences. House mice of the genus *Mus* represent an especially powerful model system for studying the interplay of PAR function and evolution from this perspective. The pseudoautosomal boundary (PAB) has been subject to considerable repositioning across the *Mus* phylogeny, including significant PAR divergence between interfertile taxa. Within the *Mus musculus* species complex, two closely related subspecies, *M. musculus domesticus* and *M. m. castaneus*, are characterized by a ~430-kb shift in the PAB (White *et al.* 2012a). The *M. m. domesticus* PAB, which appears to coincide with that of the standard laboratory mouse strain C57BL/6J, is located ~700 kb from the distal end of the *X* chromosome in intron 3 of *Mid1* (Palmer *et al.* 1997). In contrast, the *M. m. castaneus* PAR is ~1.1-Mb long and encompasses the entire *Mid1* locus (White *et al.* 2012a). Numerous indel mutations within introns of *Mid1* further distinguish the *M. m. domesticus* and *M. m. castaneus* PARs (White *et al.* 2012a).

The marked shift in the PAB between *M. m. castaneus* and *M. m. domesticus* is associated with a reduced frequency of *X/Y* synapsis in spermatocytes from F_1 hybrids (White *et al.* 2012b). Whereas 95% of heterogametic sex chromosomes are synapsed along their PARs at late pachytene in both *M. m. castaneus* and *M. m. domesticus*, the *X* and *Y* are synapsed in only ~70% of F_1 spermatocytes at this early meiotic substage. Surprisingly, however, reduced *X/Y* synapsis does not appear to elicit downstream consequences for F_1 hybrid fertility. F_1 animals have testis weights, sperm densities, and measures of sperm morphology that are comparable to or exceed fertility parameters in the inbred parental strains (White *et al.* 2012b). These findings are in line with observations from other intersubspecies house mouse hybrids, in which the *X* and *Y* experience premature dissociation at metaphase I, without obvious repercussions for male fertility (Imai *et al.* 1981; Matsuda *et al.* 1982, 1983). However, given the established significance of synapsis and recombination for meiotic progression, it remains puzzling that organisms with impaired meiotic sex chromosome associations suffer no apparent fitness consequences. One possible explanation is that animals with reduced *XY* pairing exhibit subtle spermatogenic defects, but that the associated reduction in fertility is matched or exceeded by fitness gains associated with outbreeding. A second alternative is that the resulting gametes are of reduced genetic quality, harboring elevated rates of sex chromosome aneuploidy.

Here, I apply cytogenetic methods and immunofluorescence imaging to conduct an in-depth study of sex chromosome synapsis, recombination, meiotic progression, and aneuploidy in *M. m. domesticus*, *M. m. castaneus*, and their reciprocal intersubspecific F_1 hybrids. My findings reveal the phenotypic consequences of PAR divergence on *X/Y* dynamics at meiosis, with important implications for our understanding of the functional constraints governing the evolution of the heterogametic mammalian sex chromosomes.

Materials and Methods

Animal husbandry

Wild-derived inbred strains CAST/EiJ (CAST; *M. m. castaneus*) and WSB/EiJ (WSB; *M. m. domesticus*) were purchased from The Jackson Laboratory and housed in the Biological Resources Facility at North Carolina State University according to animal care protocols approved by the North Carolina State University Animal Care and Use Committee (Protocol 13-109-B). Mice were provided with food (PicoLab Mouse Diet 20 5058*) and water *ad libitum*. Sexually mature males from each inbred strain and F_1 males from intersubspecific crosses were killed by exposure to CO_2 at 8–42 weeks of age.

Spermatocyte cell spreads and immunostaining

Meiotic cell spreads were prepared using the method of Peters *et al.* (1997) with minor modifications as described (Dumont *et al.* 2015). Spermatocyte cell spreads were immunostained according to a protocol adapted from Anderson *et al.* (1999) and Koehler *et al.* (2002) as previously described (Dumont *et al.* 2015). The primary antibodies used were as follows: mouse anti-MLH1 (1:100 dilution; BD Biosciences), goat anti-SYCP3 (1:100 dilution; Santa Cruz Biotechnology), rabbit anti-phospho-histone H2A.XpSer139 (1:1000 dilution; Thermo Scientific), human anti-centromere (1:100 dilution; Antibodies Incorporated), and rabbit anti-SYCP1 (1:100 dilution; Abcam). The following secondary antibodies were used at 1:200 concentration: donkey anti-goat Rhodamine Red-X, donkey anti-rabbit Alexa Fluor 488, donkey anti-human Aminomethylcoumarin Acetate, and donkey anti-mouse Alexa Fluor 488 (Jackson ImmunoResearch).

Fluorescent in situ hybridization analysis of the house mouse PAR

The dynamics of *X/Y* associations in early meiosis were monitored by direct labeling of PAR DNA in surface-spread spermatoctyes. Coverslips were removed from previously immunostained slides by soaking in PBS at 37° for ~1 hr. Slides were then washed briefly in 1× PBS with 0.1% Triton X-100 and dehydrated in a 70, 90, 100% ethanol series at room temperature. Slides were denatured in 70% formamide with 0.6× SSC at 73° for 7 min and then immediately processed through a second ethanol series (70, 90, 100% ethanol).

Labeled probes were synthesized from BAC clones spanning the PAR (RP24-500I4) and an *X*-linked region just outside the *M. m. domesticus* PAR (RP23-154O12) (Barchi *et al.* 2008; Kauppi *et al.* 2011). High quality BAC DNA was isolated from a 10-ml liquid culture with a BACMAX DNA purification kit following manufacturer's protocols. BAC DNA was then digested with DNaseI (1:100 dilution) and labeled with fluorescein-12-dUTP or Aqua-431-dUTP via nick translation (Enzo Life Sciences). Labeled reaction products were size verified by agarose gel electrophoresis and ranged from 200 to 1000 bp.

For each hybridization reaction, ~10–20 ng of each labeled probe was ethanol precipitated overnight at −20° in the presence of NaOAc and 1 μg mouse Cot-1 DNA (Invitrogen, Carlsbad, CA). Probes were resuspended in 10 μl of hybridization buffer [5 μl formamide, 2 μl 50% w/v dextran sulfate, 2 μl 10× SSCP (1.5 M sodium chloride, 0.15 M sodium citrate, 0.2 M sodium dihydrogen phosphate, pH = 6.0), 1 μl/μg mouse Cot-1 DNA]. The probe mix was denatured at 73° for 5 min, then allowed to renature at 37° for ~45 min. Texas-Red-labeled *Y*-chromosome paint probes (Cytocell) were denatured at 80° for 10 min following vendor recommendations. A 5 μl volume of the *Y* paint was added to the renatured BAC probes and the combined probe-paint mixture directly applied to the denatured and dehydrated spermatocyte spreads. The probed area was coverslipped, sealed with rubber cement, and incubated for 24–48 hr in a 37° humid chamber. After hybridization, the coverslip was gently removed and the slide was briefly washed in 0.4× SSC with 0.2% Tween 20 followed by a second wash in 2× SSC with 0.2% Tween 20. The slide was then rinsed with distilled water, air dried in the dark, and mounted in ProLong Gold Antifade media (Promega, Madison, WI).

Testis histology

Whole testes were submerged in Bouin's fixative overnight at 4° and washed in an ethanol series (5 min each in 25 and 50% and three successive 5 min washes in 70% ethanol). Fixed tissues were then paraffin embedded, cross-sectioned at 5 μm, and regressively stained with Mayer's Hematoxylin and Eosin-Y. Stained slides were scanned at 20× magnification with a NanoZoomer 2.0HT digital slide scanning system. Stage XII tubules were identified by the presence of meiotic cell divisions (Ahmed and de Rooij 2009). The area of each stage XII tubule was approximated using the standard equation for the area of an ellipse, πab, where a and b are the radii.

Sperm extraction and fixation

The protocol for sperm extraction and fixation was modified from Sarrate and Anton (2009). First, both cauda epididymides were dissected and placed in a 500-μl droplet of modified bovine gamete medium 3 (3.11 mM KCl, 0.3 mM NaH_2PO_4, 87 mM NaCl, 0.4 mM $MgCl{\cdot}6H_2O$, 21.6 mM sodium lactate, 1.0 mM sodium pyruvate, 10 mM $NaHCO_3$, 40 mM HEPES, 6 mg/ml bovine serum albumin, pH = 7.54) (Vredenburgh-Wilberg and Parrish 1995). The epididymides were macerated with dissecting scissors and sperm were allowed to diffuse out of the tissue into solution for 20–30 min at room temperature.

The sperm solution was then transferred to a microcentrifuge tube and pelleted by centrifugation for 10 min at 1000 × *g*. The supernatant was carefully removed and the sperm pellet was resuspended in ~1 ml of freshly prepared Carnoy's fixative that was added drop by drop with continuous, gentle mixing. Several drops of fixed sperm were dispensed onto the center of a 3- × 1-in. glass slide. Slides were allowed to air dry overnight and stored at −20° for at least 48 hr prior to hybridization.

Whole chromosome painting on sperm

Sperm slides were painted with FITC and Texas-Red-labeled whole chromosome probes targeting the *X* and *Y* chromosomes (Cytocell). Hybridizations were performed with both color-swap combinations using the method of Sarrate and Anton (2009). Briefly, sperm slides were removed from −20° storage and immediately placed into two consecutive washes in 2× SSC for 3 min each. Slides were then transferred through a series of three ethanol washes (70, 90, and 100%) for 2 min at each concentration. After air drying, sperm DNA was decondensed by immersion in a fresh dithiothreitol solution (5 mM 1,4-dithiothreitol, 1% Triton X-100, 50 mM Tris) at room temperature for 12–15 min. Slides were then soaked in two consecutive washes of 2× SSC for 3 min each, transferred

through an ethanol series for a second time (70, 90, 100% ethanol), and air dried.

Sperm DNA was denatured in 70% formamide with 2× SSC at 78° for 5 min. Slides were then transferred through an ethanol series (70, 85, 100% ethanol) for 1 min at each dilution and air dried. Whole chromosome probes were denatured for 10 min at 80° per vendor recommendations. A total volume of 10 μl of denatured probe mix was dispensed on each slide. The probed area was sealed with an 18- × 18-mm square glass coverslip and sealed with rubber cement. Slides were hybridized for ~48 hr at 37°.

After removing coverslips, slides were washed for 2 min in 0.4× SSC with 0.3% NP-40 at 74° followed by a final wash in 2× SSC with 0.1% NP-40 at room temperature for 1 min. Slides were then counterstained in DAPI, air dried in the dark, and mounted.

Fluorescent microscopy and image analysis

Slides were visualized using either a Leica DM5500 B microscope equipped with a Photometrics CoolSNAP HQ^2 charge-coupled device (CCD) camera linked to Leica Application Suite (version 2.3.5) software or an Olympus BX61 epifluorescence microscope with a cooled CCD camera linked to Smart Capture 3 software. Images were postprocessed and analyzed with the Fiji software package (Schindelin *et al.* 2012).

For MLH1 immunostained spermatocyte cell spreads, ~50 late-pachytene cells characterized by (i) the complete merge of SYCP3 signals from all autosomal homologs, (ii) a full complement of chromosomes, and (iii) minimal background fluorescence were imaged for each genotype. Cells that were damaged during preparation or displayed bulbous chromosome termini (indicative of transition into early diplotene) were not imaged. I considered only those cells with at least one clearly stained MLH1 focus on each autosomal synaptonemal complex (SC), excepting the possibility of one achiasmate bivalent. Cells with two or more SCs lacking an MLH1 focus were extremely rare and likely represented staining artifacts.

For the *X*- and *Y*-chromosome-painted sperm slides, only those visual fields with brightly stained and nonoverlapping sperm were imaged. Images with more than one aneuploid sperm cell per visual field or high levels of background fluorescence were discarded. Approximately 1500 sperm were analyzed per genotype over both dye-swap probe color combinations. The aneuploidy rate was estimated as twice the frequency of diploid *XY* sperm.

Statistical analyses

Statistical analyses were performed in the R environment for statistical computing using base packages (R Core Team 2013). The *X/Y* pairing status of analyzed spermatocytes and the aneuploidy status of all sperm cells were encoded as binary indicator variables. Distributions were compared using conservative nonparametric Mann–Whitney *U*-tests (MWU). In addition, an *ad hoc* permutation test was used to evaluate the difference in the frequency of MLH1 foci on the paired PAR between the parental strains and F_1. Briefly, I

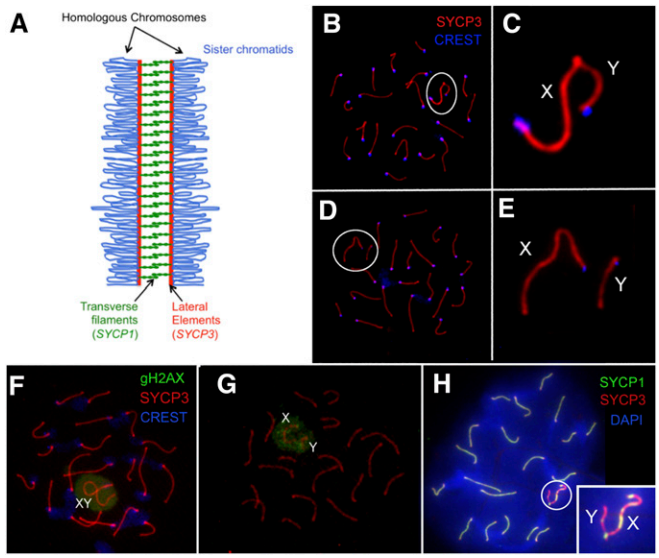

Figure 1 Sex chromosome synapsis in spermatocyte cell spreads. (A) Schematic of the mature SC composed of both lateral elements and transverse filaments. The SC serves as a scaffold for the attachment and organization of chromatin loops in meiosis I. (B) Pachytene spermatocyte immunostained for SYCP3, a component of the lateral elements of the SC, and kinetochore-associated proteins visualized by CREST antibodies. Synapsis of the sex chromosomes (circled) is restricted to the PAR (C). (D and E) Pachytene spermatocyte with asynapsed sex chromosomes. The histone modification γH2AX is limited to the sex body at pachytene, revealing transcriptional repression of sex chromatin in spermatocytes with both (F) synapsed and (G) asynapsed sex chromosomes. (H) The transverse filament protein SYCP1 is incorporated into the mature SC of the autosomes, as well as the PAR, indicating that a mature tripartite SC is assembled at the PAR when *X*- and *Y*-linked homologous regions synapse.

randomly sampled n_1 and n_2 observations from the union of both the parental and F_1 data sets, where n_1 and n_2 correspond to the actual numbers of analyzed spermatocytes with paired sex chromosomes from parental strains and F_1's. The difference in the frequency of MLH1 foci between the two randomly generated data sets was calculated and used as the test statistic. This procedure was repeated 1000 times to generate a null distribution of differences in PAR MLH1 frequency between the two data sets. The empirical *P*-value was calculated as the quantile position of the observed difference in the fraction of paired *X/Y* chromosomes with a PAR MLH1 focus along this null distribution.

Simulations were performed to assess the power to find statistically significant differences in aneuploidy frequency for variable numbers of analyzed sperm (n) and nondisjunction frequencies (f). For a given parameter combination $\{n, f_1, f_2\}$, two simulated samples of n random variables were generated assuming binomial success probabilities f_1 and f_2. The two-sided *P*-value from a MWU comparing these two distributions was then calculated and retained. The power to detect a significant difference between nondisjunction rates f_1 and f_2 when n sperm are analyzed was calculated as the fraction of 1000 simulated replicates with MWU $P < 0.05$. These simulation results are presented graphically in Supplemental Material, Figure S3.

Table 1 The fraction of pachytene spermatocytes with synapsed sex chromosomes

Strain	Animal	No. spermatocytes	Merged SYCP3 signals	SYCP1/SYCP3 colocalization
WSB	1	69	0.957	0.913
CAST	1	75	0.973	0.921
	2	36	1.00	0.972
	3	52	0.981	0.960
	4	43	0.902	0.854
	Total	**206**	**0.966**	**0.926**
WSB×CAST F_1	1	24	0.833	0.708
	2	46	0.761	0.739
	Total	**70**	**0.786**	**0.729**
CAST×WSB F_1	1	28	0.714	0.679
	2	27	0.778	0.777
	3	30	0.700	0.700
	Total	**85**	**0.729**	**0.718**

Data availability

The authors state that all data necessary for confirming the conclusions presented in the article are represented fully within the article.

Results

Cytogenetic analysis of XY pairing and synapsis at pachytene

The SC is a structural protein complex that physically tethers homologous chromosomes at meiosis. It is comprised of lateral elements that align along the chromosome axes and transverse filaments that link the lateral elements, much like the teeth of a zipper (Figure 1A) (Page and Hawley 2004). The sequential assembly of the SC during early meiosis can be tracked by immunofluorescent staining of SYCP3, a key protein component of the lateral elements, and SYCP1, a component of the transverse filaments. At leptotene, SYCP3 begins to accumulate in isolated patches along the condensing chromosome axes. As meiosis progresses, SYCP3 signals coalesce into contiguous strands that extend along the full axis of each chromosome. At pachytene, SYCP3 signals from homologous chromosomes merge and are secured along their full length by transverse filaments. This final step in the assembly of the mature SC is marked by the colocalization of SYCP3 and SYCP1 signals.

Intersubspecific F_1 hybrids derived from controlled laboratory crosses between WSB, a wild-derived inbred strain of *M. m. domesticus*, and CAST, a wild-derived inbred strain of *M. m. castaneus*, were previously shown to exhibit a reduction in the frequency of *X/Y* synapsis at late pachytene relative to the inbred parental strains (White *et al.* 2012a). Here, I validate this finding by quantifying the fraction of pachytene cells with merged SYCP3 signals at *X*- and *Y*-linked PARs in spermatocytes from both parental and F_1 genetic backgrounds (Figure 1, A–E, and Table 1). Although the *X* and *Y* chromosomes are always observed in close spatial proximity (*i.e.*, they are likely paired), the frequency of synapsis is significantly reduced in the two reciprocal F_1 genotype backgrounds relative to the parental inbred strains (Table 1; MWU $P = 5.29 \times 10^{-11}$). There is no difference in the frequency of *X/Y* synapsis between the two reciprocal F_1 backgrounds (MWU $P = 0.4203$), suggesting that this effect is a general consequence of the divergent *X*- and *Y*-linked PARs in hybrids.

In line with an earlier report (Barchi *et al.* 2008), I find no evidence for disrupted sex body formation in hybrids with unsynapsed sex chromosomes (Figure 1, F and G). A diffuse cloud of γH2AX paints the sex chromosomes in all CAST, WSB, and F_1 spermatocytes examined, indicating proper transcriptional silencing of *X*- and *Y*-linked genes (Turner *et al.* 2004) regardless of synapsis status.

When *X*- and *Y*-linked PARs do synapse in F_1 hybrids, the resulting SC almost always incorporates the transverse element protein SYCP1, indicating the formation of a mature, tripartite structure (Figure 1H and Table 1). In 93% of WSB×CAST F_1 and 98% of CAST×WSB F_1 pachytene spermatocytes with merged *X*- and *Y*-associated SYCP3 signals, SYCP1 and SYCP3 are coexpressed along the paired region. These percentages are comparable to observations for spermatocytes from the two inbred parental strains (Table 1; MWU $P = 0.84$), suggesting that structural or sequence-level divergence between the CAST and WSB PARs does not interfere with structural assembly of the full SC.

Curiously, expression of SYCP1 is not restricted to the homologous PAR pairing region, confirming previously reported patterns (Page *et al.* 2006a; Manterola *et al.* 2009). Patches of SYCP1 were commonly observed along the unsynapsed *X* and *Y* chromosome axes of all animals (Figure 1H). These regions may correspond to areas of self-synapsis mediated by tandem duplicated sequences on the *X* and *Y* or zones of nonspecific SYCP1 expression.

Sex chromosome dynamics throughout prophase I

The marked reduction in sex chromosome synapsis at pachytene in intersubspecific F_1 hybrids could be explained by (i) the failure of pairing and synapsis to occur between divergent PARs, (ii) a delay in the onset of sex chromosome synapsis, or (iii) the premature release of pairing associations initiated at earlier meiotic stages. To distinguish between these possible explanations, I monitored sex chromosome associations across the PAR in spermatocytes throughout prophase I.

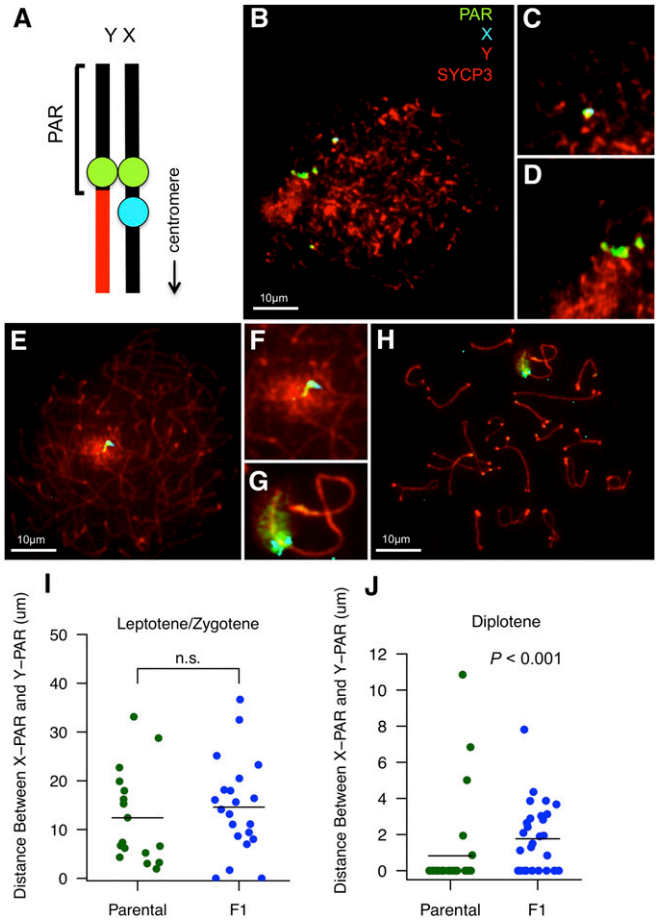

Figure 2 Combined immunofluorescence-FISH analysis of sex chromosome pairing throughout prophase I. (A) Schematic illustrating the position of fluorescently labeled probes along the *X* and *Y* chromosomes. Representative (B) leptotene-, (E) zygotene-, and (H) diplotene-stage cells immunostained for SYCP3 and subsequently FISH'ed for the PAR, *X* chromosome sequence, and a *Y* chromosome paint. Bar, 10 μm. An enlargement of the *X*-linked PAR from (B) is shown in (C) and an enlargement of the *Y*-linked PAR is shown in (D). (F) and (G) show enlargements of the paired sex chromosomes in (E) and (H), respectively. The distribution of distances between *X*- and *Y*-linked PAR sequences for the parental strains and the reciprocal F_1's at points prior to (I) and after (J) pachytene are shown. n.s., not significant.

In early prophase I, the sex chromosomes are not uniquely identifiable based on SYCP3 signals alone. This consideration necessitates use of labeled probes specific to the PAR to directly visualize the relative positions of *X*- and *Y*-linked homologous regions in a cell. By combining immunofluorescence imaging of SYCP3 with fluorescently tagged probes that hybridize to the PAR and unique regions of the *X* and *Y* chromosomes, I monitored the spatial relationship between *X*- and *Y*-linked PARs in early meiosis. Notably, there is no difference in the physical distance between *X*- and *Y*-linked PARs in surface-spread leptotene and zygotene spermatocytes from the parental and hybrid backgrounds (MWU $P = 0.25$; Figure 2I). The early chromosome movements that set the stage for pairing and synapsis are evidently not disrupted in hybrids, suggesting that PAR divergence does not interfere with the initiation of sex chromosome pairing.

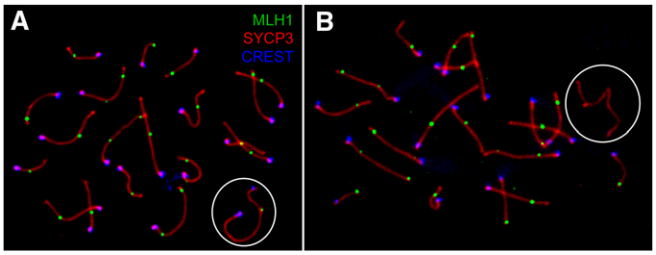

Figure 3 Frequency of MLH1 foci on the synapsed PAR at late pachytene. Late pachytene spermatocyte spreads were stained for SYCP3, CREST, and MLH1, a mismatch repair protein that localizes in discrete foci to sites of crossing over along the SC at late pachytene. Synapsed sex chromosomes are indicated by white circles. At this meiotic substage, a subset of spermatocytes harbor an MLH1 focus along the (A) synapsed PAR, with the remainder lacking a focus in this interval (B).

I next sought to determine whether the high rate of *X/Y* asynapsis in F_1 hybrids could be attributed to delayed synapsis between divergent *X*- and *Y*-linked PARs. At diplotene, the *X* and *Y* remain synapsed across the PAR in most spermatocytes from the parental strains (87%, $n = 31$ cells). In contrast, only one-third (38%, $n = 29$ cells) of sex chromosomes are synapsed in F_1's at this stage in late prophase I (MWU $P < 0.001$; Figure 2J). Thus, *X/Y* synapsis does not simply occur at a later meiotic time point in hybrids.

Taken together, these results suggest two complementary explanations for the increased frequency of *X/Y* asynapsis in intersubspecific F_1's. Although the onset of sex chromosome pairing is not affected in hybrids, divergence between *X*- and *Y*-linked PARs does appear to interfere with synapsis across this critical region as reflected in the reduced frequency of *X/Y* synapsis at pachytene (Table 1). The increased fraction of dissociated *X* and *Y* chromosomes at diplotene relative to the pachytene substage further indicates that when the *X* and *Y* do synapse, synaptic associations are often not maintained through prophase I.

Immunofluorescent analysis of PAR recombination at late pachytene

Meiotic crossovers lock homologous chromosomes together until their segregation at anaphase I. The failure of many sex chromosome pairs to remain synapsed through diplotene raises the possibility that divergent *X*- and *Y*-linked PARs often fail to secure a crossover, leading to premature separation of the heterologous *X* and *Y* chromosomes. In line with this interpretation, White *et al.* (2012b) tracked the inheritance of PAR-linked genetic markers to estimate that ~80% of inherited *Y* chromosomes in a CAST×WSB and WSB×CAST intercross F_2 population were nonrecombinant, implying that only ~40% of paired bivalents had a crossover in the PAR. However, owing to incomplete marker coverage across the region, the possibility of tight double crossovers, and potential biases in the transmission of recombinant chromosomes, this fraction may be an underestimate of the true value. To overcome these limitations, I estimated crossover frequency by direct cytogenetic visualization of the mismatch repair protein MLH1 on the paired sex chromosomes at pachytene (Figure 3).

Table 2 Frequency of MLH1 foci on synapsed sex chromosomes in late-pachytene spermatocytes

Strain	Animal	Total no. spermatoctyes	No. spermatocytes with synapsed *X/Y*	Fraction of spermatocytes with MLH1 focus on the PAR (±95% C.I.)[a]
WSB		41	40	0.63 (0.45–0.75)
CAST		59	56	0.43 (0.29–0.55)
WSB×CAST F_1	1	28	19	0.26 (0.05–0.37)
	2	20	12	0.25 (0–0.33)
	3	22	18	0.39 (0.11–0.56)
	Total	**70**	**49**	**0.31 (0.10–0.33)**
CAST×WSB F_1	1	22	12	0.25 (0–0.33)
	2	29	22	0.41 (0.14–0.50)
	Total	**51**	**34**	**0.35 (0.11–0.41)**

[a] Considering only the subset of spermatoctyes with synapsed *X/Y* chromosomes.

The dynamics of the sex chromosomes and autosomes are decoupled during meiosis, with the steps of *X/Y* pairing, synapsis, and recombination operating on a temporal lag relative to the autosomes (Kauppi *et al.* 2011). Although the frequency of MLH1 foci at late pachytene approximates the autosomal distribution of crossovers (Anderson *et al.* 1999; Koehler *et al.* 2002), MLH1 foci observed on the PAR at this meiotic substage may not provide an accurate read out of the absolute crossover rate between the *X* and *Y*. Indeed, I observed an MLH1 focus on the PAR in only ~50% of parental CAST and WSB spermatocytes at late pachytene (Table 2), despite the presumed ubiquity of crossing over in this region and the presence of one or more MLH1 foci on each autosomal bivalent. This percentage matches observations from other inbred house mouse strains and wild-caught outbred house mice (Dumont and Payseur 2011), suggesting that only a subset of PAR crossovers are resolved synchronously with the autosomes in house mice. Importantly, there is no difference in the mean number of autosomal MLH1 foci between spermatocytes with an MLH1 focus on the synapsed PAR *vs.* those with no MLH1 focus in this interval (MWU $P > 0.3$ for all genetic backgrounds; Figure S1). Although modest sample sizes may limit the power to detect subtle effects, these two classes of spermatocytes appear to be isolated from comparable time points in pachytene.

I used the fraction of late-pachytene spermatocytes with an MLH1 focus along the paired PAR as a proxy for the *relative* rate of recombination across this locus. Approximately one-third of F_1 spermatocytes with a full complement of autosomal MLH1 foci also have a focus on the PAR (Table 2). This constitutes a 25% reduction over the fraction of spermatocytes with an MLH1 focus on the PAR in either inbred WSB or CAST at this same meiotic stage. This difference is not significant by the statistically conservative two-tailed MWU ($P = 0.104$), but does exceed the significance threshold of a less stringent *ad hoc* permutation test ($P = 0.041$; see *Materials and Methods*). Whether the slight decrease in recombination frequency in hybrids is due to reduced formation of double-strand breaks (DSBs) in this region or a reduction in the ratio of DSBs that are repaired as crossovers remains unclear. Regardless of the underlying mechanism, nearly half of all spermatoctyes from intersubspecific F_1 males are characterized by unsynapsed or achiasmate sex chromosomes.

Apoptosis at meiosis I in hybrid spermatocytes

Prior studies have established that asynapsed or achiasmate chromosomes can activate the spindle checkpoint, causing cells to arrest at metaphase I (Burgoyne *et al.* 2009; Gorbsky 2014). Given the high frequency of misbehaved *X/Y* chromosomes in CAST and WSB hybrids, I reasoned that F_1 animals should exhibit an elevated frequency of cell death at meiosis I relative to the parental strains. To test this idea, I performed histological analysis of stage XII seminiferous tubules in testis cross-sections (Figure 4). Tubules at this stage of spermatogenesis are characterized by the presence of meiotically dividing cells discernable by their conspicuous chromatin staining patterns (Ahmed and de Rooij 2009).

Adult WSB males exhibited extensive vacuolization of the seminiferous tubules at multiple stages of spermatogenic progression (Figure S2), consistent with a prior report (Odet *et al.* 2015). Given the aberrant-testis phenotype in this parental strain, I focused on the contrast between both reciprocal F_1's and CAST. Over 90% of stage XII tubules from CAST×WSB and WSB×CAST F_1's contain metaphase I cells with darkened, eosinophilic cytoplasm, indicative of cell death (Figure 4 and Table 3). In contrast, <6% of stage XII tubules from CAST males harbor one or more apoptotic cells (Table 3). The increased rate of cell death during CAST×WSB F_1 spermatogenesis is associated with a decreased average tubule size relative to the inbred CAST strain, presumably reflecting a depletion of postmeiotic cells (Table 3). There is no difference in mean tubule area between CAST and WSB×CAST F_1's (MWU $P = 0.4029$), despite the significantly greater number of apoptotic cells in tubules from these F_1 hybrids.

Rates of sex chromosome aneuploidy in parental and hybrid backgrounds

Although a subset of spermatocytes with synaptic defects is eliminated at meiosis I, I speculated that reduced PAR recombination and the impaired *X/Y* dynamics observed in WSB and CAST F_1 hybrids may render the *X* and *Y* liable to nondisjunction in the subset of spermatoctyes that do progress through the first meiotic division. To test this hypothesis, I used *X*- and *Y*-chromosome painting on sperm to assess the sex chromosome content of >1500 sperm isolated from CAST, WSB, and reciprocal F_1 male mice. A

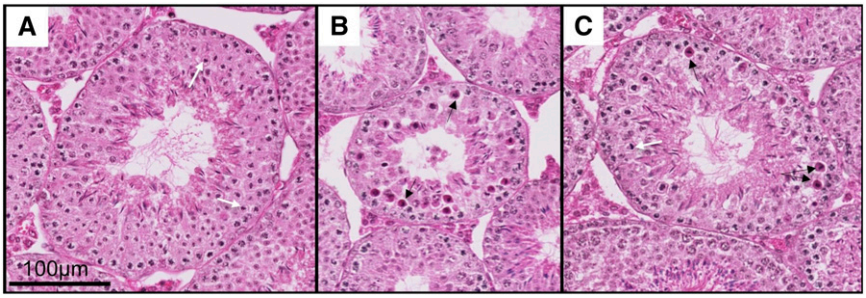

Figure 4 Increased apoptosis in meiotic cells from intersubspecific F_1's. Hematoxylin- and Eosin-Y-stained testis cross-sections from (A) CAST/EiJ, (B) CAST×WSB F_1, and (C) WSB×CAST F_1 adult male mice. Tubules are at stage XII of the seminiferous epithelial cycle. There are multiple meiotically dividing cells with darkened, eosinophilic cytoplasm in tubules from F_1 backgrounds (black arrows), indicative of cell death. In contrast, meiotically dividing cells in CAST/EiJ were rarely apoptotic (white arrows). Despite the higher rate of apoptosis in F_1's, a subset of cells do progress through meiosis, evidenced by the presence of postmeiotic elongating spermatids in seminiferous tubules from these genetic backgrounds. Bar, 100 μm. Images are equally scaled.

representative image of this assay is shown in Figure 5. Despite the statistical power to find an approximately threefold difference in aneuploidy rate (Figure S3), the frequencies of sex chromosome aneuploid sperm in F_1 hybrids and the inbred parental strains are statistically indistinguishable (MWU $P = 0.3857$; Table 4).

Intriguingly, there is a ~3.5-fold difference in the *XY* sperm aneuploidy rate between mice with a CAST-derived *X* chromosome (CAST and CAST×WSB F_1's; aneuploid fraction = 0.0085; Table 4) and mice with the WSB-derived *X* chromosome (WSB and WSB×CAST F_1's; aneuploid fraction = 0.0025; MWU $P = 0.0197$). This observation links the CAST *X* chromosome to a higher rate of sex chromosome nondisjunction.

Discussion

PAR divergence and meiotic progression in house mice

M. m. castaneus and *M. m. domesticus* are characterized by a pronounced shift in the PAB and numerous small structural differences across their PARs (White *et al.* 2012a). In an effort to define the meiotic consequences of this PAR divergence, I used cytogenetic approaches to directly visualize sex chromosomes in spermatocytes from intersubspecific F_1 hybrids. I demonstrated that the frequency of sex chromosome pairing and synapsis at meiosis is markedly reduced in hybrids. Among the subset of F_1 spermatocytes with synapsed sex chromosomes, synaptic associations were commonly prematurely released. Moreover, I observed a ~25% reduction in the rate of recombination across the paired region in hybrids relative to the inbred parental strains. Net, I estimate that upward of 50% of spermatocytes in F_1 hybrids fall short of the stereotyped demands for *X/Y* synapsis and recombination at meiosis.

Although these defects in *X/Y* synapsis and recombination are associated with meiotic arrest, F_1's are fertile, exhibiting testis weights and sperm densities comparable to or exceeding the parental values (White *et al.* 2012b). These findings recapitulate observations in hybrids between other house mouse subspecies. Upward of 60–80% of spermatocytes from *M. m. molossinus* and C57BL/6J hybrids (Imai *et al.* 1981), and F_1 hybrids between wild-caught *M. musculus* animals and inbred laboratory strains of predominately *M. m. domesticus* ancestry (Yang *et al.* 2007) display premature dissociation of the *X* and *Y* at metaphase I, without clear repercussions for fertility or nondisjunction (Matsuda *et al.* 1982). Collectively, these findings seem to underscore the severity of inbreeding depression in inbred mouse strains. The fitness increase associated with a single generation of outcrossing can evidently compensate for errors in synapsis and recombination affecting a substantial fraction of F_1 spermatocytes, resulting in no net loss of fertility compared to the parental strains. However, even though the level of PAR divergence tested here does not overtly decrease hybrid fitness in the laboratory setting, the consequences of divergent *X*- and *Y*-linked PARs on reproductive fitness in natural, wild populations could be substantial.

Taken together, these results clearly indicate that some level of structural and sequence divergence between *X*- and *Y*-linked PARs is compatible with meiotic progression and fertility. However, the baseline level of homology and minimum PAR length required for meiotic progression remain unknown. Evidently, divergence between CAST and WSB PARs falls within the permissive range, as many spermatocytes progress through meiosis. In contrast, F_1 hybrids between C57BL6/J and *M. spretus* possess more divergent *X*- and *Y*-linked PARs that almost invariably fail to synapse and males are completely sterile (Matsuda *et al.* 1991, 1992). However, owing to the complexity of hybrid sterility in these divergent interspecific hybrids (Hale *et al.* 1993; Oka *et al.* 2010), it is not clear whether *X/Y* asynapsis *per se* is the underlying cause of sterility.

Although there is a pronounced shift in the PAB between *M. m. domesticus* and *M. m. castaneus*, data on finer-scale structural differences and sequence diversity in the PARs of these subspecies is limited to regions near the boundary (White *et al.* 2012a), which may not be representative of patterns across the full PAR. Indeed, the PAR is one of the most understudied regions of the genome. Whole genome sequences are now available for >100 mammalian species, but *X*- and *Y*-linked PAR sequences are available for only 8 (Bellott *et al.* 2014). The PAR is known to harbor considerable diversity among individuals (Kipling *et al.* 1996; Mensah *et al.* 2014), but the full scope of within-population genetic variation across the full locus remains unsurveyed. The absence of comprehensive sequence data from this genomic interval presents an obstacle to understanding how the sequence content and patterns of homology between *X*- and *Y*-linked PARs influence the

Table 3 Histological analysis of stage XII tubules

Strain	Animal	No. of stage XII tubules examined	Mean tubule size (mm^2)	Fraction stage XII tubules with apoptotic cells
CAST	1	6	0.335	0.167
	2	7	0.292	0
	3	5	0.374	0
	Total	**18**	**0.328**	**0.056**
CAST×WSB F_1	1	12	0.201	0.917
	2	10	0.225	1
	3	11	0.229	0.909
	4	5	0.230	1
	Total	**48**	**0.220**	**0.938**
WSB×CAST F_1	1	8	0.337	0.875
	2	5	0.283	1
	3	6	0.387	1
	Total	**19**	**0.327**	**0.947**

meiotic function of this locus. Emerging single molecule, long-read DNA sequencing technologies may offer a solution to decoding patterns of fine-scale diversity across the PAR, enabling investigation of the molecular conditions that must be upheld for divergent *X*- and *Y*-linked PARs to pair, synapse, and recombine at meiosis.

In addition to divergence between *X*- and *Y*-linked PAR sequences, the meiotic function of the PAR may be influenced by genetic interactions with other loci (Imai *et al.* 1981; Matsuda *et al.* 1983). Indeed, White *et al.* (2012b) detected several epistatic interactions between autosomal variants and PAR-linked loci that contribute to multiple measures of hybrid sterility in CAST and WSB F_2's. Although speculative, PAR-associated sterility in advanced generation hybrids could also depend on the inheritance of sex chromosomes that have passaged through at least one hybrid meiosis. In particular, there is evidence for genetic destabilization of the *X* and *Y* chromosomes in house mouse hybrids (Scavetta and Tautz 2010), a phenomenon that could engender structural rearrangements that further disrupt homology across the PAR in later hybrid generations.

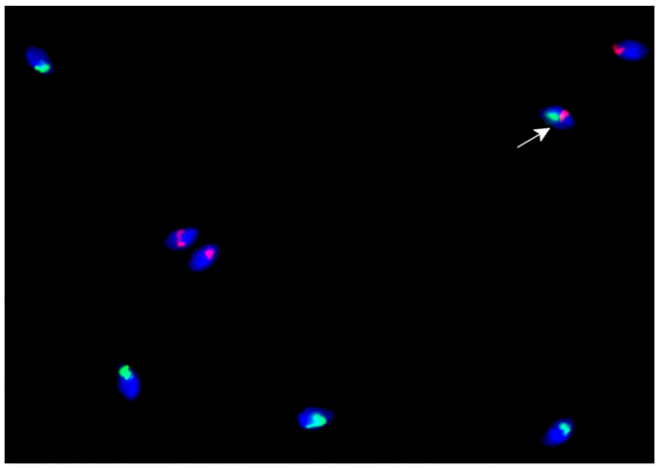

Figure 5 Aneuploidy rate estimated by whole chromosome painting on sperm. The sex chromosome constitution of single sperm assayed by whole chromosome painting. Aneuploid *XY* sperm are identified by the presence of signals from *X* and *Y* probes (arrow).

Diversity of XY segregation mechanisms in mammals and long-term evolutionary prospects for the murine PAR

Although synapsis and recombination are required for meiotic progression and correct *X/Y* segregation in both mice and humans (Gabriel-Robez *et al.* 1990; Hassold *et al.* 1991; Mohandas *et al.* 1992; Shi *et al.* 2001; Jorgez *et al.* 2011), these steps are not essential for sex chromosome segregation in all taxa (Page *et al.* 2006b). Noncanonical mechanisms of sex chromosome segregation have been previously described in marsupials (Solari and Bianchi 1975; Page *et al.* 2005, 2006a) and several nonmurid rodent species (de la Fuente *et al.* 2007, 2012). These exceptional species possess sex chromosomes that are fully nonhomologous—with no PAR—yet sex chromosomes segregate reductionally at the first meiotic division. In these taxa, physical linkages between the heterogametic *X* and *Y* are maintained by proteins rather than homology-driven DNA interactions (Page *et al.* 2005, 2006a; de la Fuente *et al.* 2007).

The gradual evolutionary erosion of the PAR in the ancestors of these exceptional species may have imposed selection for alternative, nonhomology-driven mechanisms of sex chromosome segregation. Once in place, such mechanisms could safeguard sex chromosome segregation against frequent errors in pairing, synapsis, and recombination, ultimately eliminating the biological need for a PAR and setting the stage for the complete loss of homology between the *X* and *Y* in these species (Blackmon and Demuth 2015).

In view of this evolutionary model, it is interesting to note that the house mouse PAR is markedly shorter than that of other mammalian species. The murine PAR measures less than half the size of the human PAR1 and only ~15% the length of the dog PAR (Young *et al.* 2008). Moreover, as demonstrated here, the house mouse sex chromosomes are highly vulnerable to asynapsis in hybrids and several *inbred* mouse strains even exhibit high levels of *X/Y* dissociation (Matsuda *et al.* 1982). The mouse PAR

Table 4 Sex chromosome genotype and *XY* aneuploidy rate in sperm

Strain	Male	No. of *X*-bearing sperm			No. of *Y*-bearing sperm			No. of *XY* diploid sperm			Frequency of sex chromosome aneuploidy (95% C.I.)[a]
		PS1	PS2	Total	PS1	PS2	Total	PS1	PS2	Total	
WSB	1	0	30	30	0	25	25	0	0	0	0 (NA)
	2	596	184	780	643	210	853	2	0	2	0.0024 (0–0.0061)
	Total	**596**	**214**	**810**	**643**	**235**	**878**	**2**	**0**	**2**	**0.0014 (0–0.0059)**
CAST	1	351	581	932	391	615	1006	8	4	12	0.0123 (0.0062–0.0195)
	2	0	67	67	0	68	68	0	0	0	0 (NA)
	Total	**351**	**648**	**999**	**391**	**683**	**1074**	**8**	**4**	**12**	**0.0115 (0.0058–0.0192)**
WSB×CAST F_1	1	172	250	422	199	244	443	0	0	0	0 (NA)
	2	106	188	294	166	168	334	0	2	2	0.0063 (0–0.0159)
	Total	**278**	**438**	**716**	**365**	**412**	**777**	**0**	**2**	**2**	**0.0027 (0–0.0067)**
CAST×WSB F_1	1	0	135	135	0	128	128	0	0	0	0 (NA)
	2	221	478	699	236	459	695	4	0	4	0.0057 (0.0014–0.0114)
	Total	**221**	**613**	**834**	**236**	**587**	**823**	**4**	**0**	**4**	**0.0048 (0.0012–0.0096)**

NA, not applicable. PS1: Probe set 1, X-Texas Red, Y-FITC. PS2: Probe set 2, X-FITC, Y-Texas Red.
[a] Computed as twice the frequency of diploid XY sperm.

may be approaching the minimum length required to drive homologous pairing and recombination, potentially rendering house mouse species poised to acquire a noncanonical sex chromosome segregation mechanism. Alternatively, the short house mouse PAR may represent an evolutionarily transient state. Mutations leading to elongation of the PAR may incur a selective advantage, ultimately driving the expansion of this region. Although additional data on PAR length variation are needed to formally test this possibility, existing data do point to a directional trend in PAR evolution in house mice. Relative to the ancestral *M. spretus* PAB, the PAB in *M. musculus* subspecies has undergone at least two proximal extension events (Perry *et al.* 2001; White *et al.* 2012a).

A toxic meiotic effect of the CAST/EiJ X chromosome

Two incidental findings to emerge from this study are the elevated frequency of sex chromosome aneuploidy and the decreased seminiferous tubule size in animals with a CAST-derived *X* chromosome (CAST and CAST×WSB F_1's) relative to male mice with a WSB-derived *X* chromosome (WSB and WSB×CAST F_1's). White *et al.* (2012b) reported a number of hybrid-sterility QTL mapping to the PAR in CAST/WSB×CAST/WSB F_2 mice, including QTL for sperm density, testis weight, sperm morphology, and seminiferous tubule area. Intriguingly, this study found no PAR-linked hybrid-sterility QTL in the reciprocal WSB/CAST×WSB/CAST F_2 population, in which males carry a WSB-derived *X* chromosome. This result, combined with the data presented here, suggests a putatively toxic meiotic effect of the CAST *X* chromosome. Segments from the CAST *X* are significantly underrepresented among genotypes from strains produced by the Collaborative Cross, an eight-way recombinant inbred panel of mice (Iraqi *et al.* 2012). Furthermore, inbred CAST males have reduced sperm counts and a high frequency of sperm morphological abnormalities (White *et al.* 2012b), hinting at meiotic defects attributable to alleles present in the inbred CAST/EiJ strain. Given the prominent role this strain plays in biomedical research and mouse genetics (*e.g.*, The Complex Trait Consortium 2004; Earle *et al.* 2012; Omura *et al.* 2015), it is of considerable interest to elucidate the basis of these observations.

Conclusions

Despite its critical homology-driven roles in mammalian meiosis, the PAR is one of the most rapidly evolving loci in the genome. Here, I have shown that genetic divergence between *X*- and *Y*-linked PARs in *M. m. castaneus* and *M. m. domesticus* intersubspecific F_1 hybrids is associated with a decreased rate of *X/Y* synapsis, reduced PAR recombination, and an elevated frequency of meiotic cell death. Despite these striking meiotic phenotypes, hybrids with mismatched *X*- and *Y*-linked PARs remain fertile, indicating some tolerance to molecular divergence across this interval. Ongoing efforts to catalog patterns of between-species divergence and within-population polymorphism across the PAR will enable inference of the evolutionary forces shaping genetic variation at this locus and provide a more refined understanding of the relationship between *X/Y* homology and PAR dynamics at meiosis.

Acknowledgments

I am grateful to two anonymous reviewers for their constructive feedback on an earlier version of this work. I thank Bret Payseur and Mike White for many thought-provoking conversations on the PAR. I thank Christina Williams and Matthew Breen for instruction on FISH methodology. I acknowledge the Anholt, Aylor, Breen, Mackay, and Singh laboratories at North Carolina State University for the use of equipment and laboratory space. This work was supported by a distinguished postdoctoral fellowship with the Initiative in Biological Complexity at North Carolina State University and a National Institute of General Medical Sciences K99/R00 Pathway to Independence award (GM-110332).

Literature Cited

Acosta, M. J., I. Romero-Fernández, A. Sánchez, and J. A. Marchal, 2011 Comparative analysis by chromosome painting of the sex chromosomes in arvicolid rodents. Cytogenet. Genome Res. 132: 47–54.

Ahmed, E. A., and D. G. de Rooij, 2009 Staging of mouse seminiferous tubule cross-sections. Methods Mol. Biol. 558: 263–277.

Anderson, L. K., A. Reeves, L. M. Webb, and T. Ashley, 1999 Distribution of crossing over on mouse synaptonemal complexes using immunofluorescent localization of MLH1 protein. Genetics 151: 1569–1579.

Baarends, W. M., E. Wassenaar, R. van der Laan, J. Hoogerbrugge, E. Sleddens-Linkels *et al.*, 2005 Silencing of unpaired chromatin and histone H2A ubiquitination in mammalian meiosis. Mol. Cell. Biol. 25: 1041–1053.

Barchi, M., I. Roig, M. Di Giacomo, D. G. De Rooij, S. Keeney *et al.*, 2008 ATM promotes the obligate XY crossover and both crossover control and chromosome axis integrity on autosomes. PLoS Genet. 4: e1000076.

Bellott, D. W., J. F. Hughes, H. Skaletsky, L. G. Brown, T. Pyntikova *et al.*, 2014 Mammalian Y chromosomes retain widely expressed dosage-sensitive regulators. Nature 508: 494–499.

Blackmon, H., and J. P. Demuth, 2015 The fragile Y hypothesis: Y chromosome aneuploidy as a selective pressure in sex chromosome and meiotic mechanism evolution. BioEssays 37: 942–950.

Borodin, P. M., E. A. Basheva, A. A. Torgasheva, O. A. Dashkevich, F. N. Golenishchev *et al.*, 2012 Multiple independent evolutionary losses of XY pairing at meiosis in the grey voles. Chromosome Res. 20: 259–268.

Burgoyne, P., 1982 Genetic homology and crossing over in the X and Y chromosomes of mammals. Hum. Genet. 61: 85–90.

Burgoyne, P. S., and E. P. Evans, 2000 A high frequency of XO offspring from X(Paf)Y* male mice: evidence that the Paf mutation involves an inversion spanning the X PAR boundary. Cytogenet. Cell Genet. 91: 57–61.

Burgoyne, P. S., S. K. Mahadevaiah, and J. M. A. Turner, 2009 The consequences of asynapsis for mammalian meiosis. Nat. Rev. Genet. 10: 207–216.

Bussell, J. J., N. M. Pearson, R. Kanda, D. A. Filatov, and B. T. Lahn, 2006 Human polymorphism and human-chimpanzee divergence in pseudoautosomal region correlate with local recombination rate. Gene 368: 94–100.

Charlesworth, B., 1996 The evolution of chromosomal sex determination and dosage compensation. Curr. Biol. 6: 149–162.

Cohen, P. E., S. E. Pollack, and J. W. Pollard, 2006 Genetic analysis of chromosome pairing, recombination, and cell cycle control during first meiotic prophase in mammals. Endocr. Rev. 27: 398–426.

de la Fuente, R., M. T. Parra, A. Viera, A. Calvente, R. Gómez *et al.*, 2007 Meiotic pairing and segregation of achiasmate sex chromosomes in eutherian mammals: the role of SYCP3 protein. PLoS Genet. 3: e198.

de la Fuente, R., A. Sanchez, J. A. Marchal, A. Viera, M. T. Parra *et al.*, 2012 A synaptonemal complex-derived mechanism for meiotic segregation precedes the evolutionary loss of homology between sex chromosomes in arvicolid mammals. Chromosoma 121: 433–446.

Dumont, B. L., and B. A. Payseur, 2011 Evolution of the genomic recombination rate in murid rodents. Genetics 187: 643–657.

Dumont, B. L., A. A. Devlin, D. M. Truempy, J. C. Miller, and N. D. Singh, 2015 No evidence that infection alters the global recombination rate in house mice. PLoS One 10: e0142266.

Earle, P. L., J. L. Americo, and B. Moss, 2012 Lethal monkeypox virus infection of CAST/EiJ mice is associated with a deficient gamma interferon response. J. Virol. 86: 9105–9112.

Filatov, D. A., and D. T. Gerrard, 2003 High mutation rates in human and ape pseudoautosomal genes. Gene 317: 67–77.

Gabriel-Robez, O., Y. Rumpler, C. Ratomponirina, C. Petit, J. Levilliers *et al.*, 1990 Deletion of the pseudoautosomal region and lack of sex-chromosome pairing at pachytene in two infertile men carrying an X;Y translocation. Cytogenet. Cell Genet. 54: 38–42.

Gorbsky, G. J., 2014 The spindle checkpoint and chromosome segregation in meiosis. FEBS J. 282: 2471–2487.

Graves, J. A. M., M. A. Ferguson-Smith, A. McLaren, U. Mittwoch, M. B. Renfree *et al.*, 1995 The evolution of mammalian sex chromosomes and the origin of sex determining genes. Philos. Trans. Biol. Sci. 350: 305–312.

Hale, D. W., L. L. Washburn, and E. M. Eicher, 1993 Meiotic abnormalities in hybrid mice of the C57BL/6J x Mus spretus cross suggest a cytogenetic basis for Haldane's rule of hybrid sterility. Cytogenet. Cell Genet. 63: 221–234.

Handel, M. A., and J. C. Schimenti, 2010 Genetics of mammalian meiosis: regulation, dynamics and impact on fertility. Nat. Rev. Genet. 11: 124–136.

Hassold, T., and P. Hunt, 2001 To err (meiotically) is human: the genesis of human aneuploidy. Nat. Rev. Genet. 2: 280–291.

Hassold, T. J., S. L. Sherman, D. Pettay, D. C. Page, and P. A. Jacobs, 1991 XY chromosome nondisjunction in man is associated with diminished recombination in the pseudoautosomal region. Am. J. Hum. Genet. 49: 253–260.

Hawley, R. S., J. A. Frazier, and R. Rasooly, 1994 Separation anxiety: the etiology of nondisjunction in flies and people. Hum. Mol. Genet. 3: 1521–1528.

Imai, H. T., Y. Matsuda, T. Shiroishi, and K. Moriwaki, 1981 High frequency fo X-Y chromosome dissociation in primary spermatocytes of F1 hybrids between Japanese wild mice (Mus musculus molossinus) and inbred laboratory mice. Cytogenet. Cell Genet. 29: 166–175.

Iraqi, F. A., M. Mahajne, Y. Salaymah, H. Sandovski, H. Tayem *et al.*, 2012 The genome architecture of the collaborative cross mouse genetic reference population. Genetics 190: 389–401.

Jorgez, C. J., J. W. Weedin, A. Sahin, M. Tannour-Louet, S. Han *et al.*, 2011 Aberrations in pseudoautosomal regions (PARs) found in infertile men with Y-chromosome microdeletions. J. Clin. Endocrinol. Metab. 96: E674–E679.

Kauppi, L., M. Barchi, F. Baudat, P. J. Romanienko, S. Keeney *et al.*, 2011 Distinct properties of the XY pseudoautosomal region crucial for male meiosis. Science 331: 916–920.

Kipling, D., H. E. Wilson, E. J. Thomson, M. Lee, J. Perry *et al.*, 1996 Structural variation of the pseudoautosomal region between and within inbred mouse strains. Proc. Natl. Acad. Sci. USA 93: 171–175.

Koehler, K. E., J. P. Cherry, A. Lynn, P. A. Hunt, and T. J. Hassold, 2002 Genetic control of mammalian meiotic recombination. I. Variation in exchange frequencies among males from inbred mouse strains. Genetics 162: 297–306.

Korobova, O., P. W. Lane, J. Perry, S. Palmer, A. Ashworth *et al.*, 1998 Patchy fur, a mouse coat mutation associated with X-Y nondisjunction, maps to the pseudoautosomal boundary region. Genomics 54: 556–559.

Lahn, B. T., and D. C. Page, 1999 Four evolutionary strata on the human X chromosome. Science 286: 964–967.

Lamb, N. E., S. B. Freeman, A. Savage-Austin, D. Pettay, L. Taft *et al.*, 1996 Susceptible chiasmate configurations of chromosome 21 predispose to non-disjunction in both maternal meiosis I and meiosis II. Nat. Genet. 14: 400–405.

Mangs, A. H., and B. J. Morris, 2007 The human pseudoautosomal region (PAR): origin, function and future. Curr. Genomics 8: 129–136.

Manterola, M., J. Page, C. Vasco, S. Berríos, M. T. Parra *et al.*, 2009 A high incidence of meiotic silencing of unsynapsed

chromatin is not associated with substantial pachytene loss in heterozygous male mice carrying multiple simple Robertsonian translocations. PLoS Genet. 5: e1000625.
Mather, K., 1938 Crossing-over. Biol. Rev. Camb. Philos. Soc. 13: 252–292.
Matsuda, Y., H. T. Imai, K. Moriwaki, K. Kondo, and F. Bonhomme, 1982 X-Y chromosome dissociation in wild derived Mus musculus subspecies, laboratory mice, and their F1 hybrids. Cytogenet. Cell Genet. 34: 241–252.
Matsuda, Y., H. T. Imai, K. Moriwaki, and K. Kondo, 1983 Modes of inheritance of X-Y dissociation in inter-subspecies hybrids between BALB/c mice and Mus musculus molossinus. Cytogenet. Cell Genet. 35: 209–215.
Matsuda, Y., T. Hirobe, and V. M. Chapman, 1991 Genetic basis of X-Y chromosome dissociation and male sterility in interspecific hybrids. Proc. Natl. Acad. Sci. USA 88: 4850–4854.
Matsuda, Y., P. B. Moens, and V. M. Chapman, 1992 Deficiency of X and Y chromosomal pairing at meiotic prophase in spermatocytes of sterile interspecific hybrids between laboratory mice (Mus domesticus) and Mus spretus. Chromosoma 101: 483–492.
Mensah, M. A., M. S. Hestand, M. H. D. Larmuseau, M. Isrie, N. Vanderheyden *et al.*, 2014 Pseudoautosomal region 1 length polymorphism in the human population. PLoS Genet. 10: e1004578.
Mohandas, T. K., R. M. Speed, M. B. Passage, P. H. Yen, A. C. Chandley *et al.*, 1992 Role of the pseudoautosomal region in sex-chromosome pairing during male meiosis: meiotic studies in a man with a deletion of distal Xp. Am. J. Hum. Genet. 51: 526–533.
Nicklas, R. B., 1974 Chromosome segregation mechanisms. Genetics 78: 205–213.
Odet, F., W. Pan, T. A. Bell, S. G. Goodson, A. M. Stevens *et al.*, 2015 The founder strains of the collaborative cross express a complex combination of advantageous and deleterious traits for male reproduction. G3 (Bethesda) 5: 2671–2683.
Oka, A., A. Mita, Y. Takada, H. Koseki, and T. Shiroishi, 2010 Reproductive isolation in hybrid mice due to spermatogenesis defects at three meiotic stages. Genetics 186: 339–351.
Omura, T., K. Omura, A. Tedeschi, P. Riva, M. W. Painter *et al.*, 2015 Robust axonal regeneration occurs in the injured CAST/Ei mouse CNS. Neuron 86: 1215–1227.
Page, J., S. Berríos, M. T. Parra, A. Viera, J. Á. Suja *et al.*, 2005 The program of sex chromosome pairing in meiosis is highly conserved across marsupial species: implications for sex chromosome evolution. Genetics 170: 793–799.
Page, J., A. Viera, M. T. Parra, R. De La Fuente, J. Á. Suja *et al.*, 2006a Involvement of synaptonemal complex proteins in sex chromosome segregation during marsupial male meiosis. PLoS Genet. 2: e136.
Page, J., R. de la Fuente, R. Gómez, A. Calvente, A. Viera *et al.*, 2006b Sex chromosomes, synapsis, and cohesins: a complex affair. Chromosoma 115: 250–259.
Page, S. L., and R. S. Hawley, 2004 The genetics and molecular biology of the synaptonemal complex. Annu. Rev. Cell Dev. Biol. 20: 525–558.
Palmer, S., J. Perry, D. Kipling, and A. Ashworth, 1997 A gene spans the pseudoautosomal boundary in mice. Proc. Natl. Acad. Sci. USA 94: 12030–12035.
Perry, J., and A. Ashworth, 1999 Evolutionary rate of a gene affected by chromosomal position. Curr. Biol. 9: 987–989.
Perry, J., S. Palmer, A. Gabriel, and A. Ashworth, 2001 A short pseudoautosomal region in laboratory mice. Genome Res. 11: 1826–1832.
Peters, A. H., A. W. Plug, M. J. van Vugt, and P. de Boer, 1997 A drying-down technique for the spreading of mammalian meiocytes from the male and female germline. Chromosome Res. 5: 66–68.
R Core Team, 2013 *R: A Language and Environment for Statistical Computing*. R Foundation for Statistical Computing, Vienna, Austria. https://www.R-project.org/.
Ross, L. O., R. Maxfield, and D. Dawson, 1996 Exchanges are not equally able to enhance meiotic chromosome segregation in yeast. Proc. Natl. Acad. Sci. USA 93: 4979–4983.
Sarrate, Z., and E. Anton, 2009 Fluorescence in situ hybridization (FISH) protocol in human sperm. J. Vis. Exp., 1405.
Scavetta, R. J., and D. Tautz, 2010 Copy number changes of CNV regions in intersubspecific crosses of the house mouse. Mol. Biol. Evol. 27: 1845–1856.
Schiebel, K., J. Meder, A. Rump, A. Rosenthal, M. Winkelmann *et al.*, 2000 Elevated DNA sequence diversity in the genomic region of the phosphatase PPP2R3L gene in the human pseudoautosomal region. Cytogenet. Cell Genet. 91: 224–230.
Schindelin, J., I. Arganda-Carreras, E. Frise, V. Kaynig, M. Longair *et al.*, 2012 Fiji: an open-source platform for biological-image analysis. Nat. Methods 9: 676–682.
Shi, Q., E. Spriggs, L. L. Field, E. Ko, L. Barclay *et al.*, 2001 Single sperm typing demonstrates that reduced recombination is associated with the production of aneuploid 24,XY human sperm. Am. J. Med. Genet. 99: 34–38.
Shiu, P. K., N. B. Raju, D. Zickler, and R. L. Metzenberg, 2001 Meiotic silencing by unpaired DNA. Cell 107: 905–916.
Solari, A. J., and N. O. Bianchi, 1975 The synaptic behaviour of the X and Y chromosomes in the marsupial Monodelphis dimidiata. Chromosoma 52: 11–25.
The Complex Trait Consortium, 2004 The collaborative cross, a community resource for the genetic analysis of complex traits. Nat. Genet. 36: 1133–1137.
Turner, J. M. A., O. Aprelikova, X. Xu, R. Wang, S. Kim *et al.*, 2004 BRCA1, histone H2AX phosphorylation, and male meiotic sex chromosome inactivation. Curr. Biol. 14: 2135–2142.
Turner, J. M. A., S. K. Mahadevaiah, O. Fernandez-Capetillo, A. Nussenzweig, X. Xu *et al.*, 2005 Silencing of unsynapsed meiotic chromosomes in the mouse. Nat. Genet. 37: 41–47.
Vredenburgh-Wilberg, W. L., and J. J. Parrish, 1995 Intracellular pH of bovine sperm increases during capacitation. Mol. Reprod. Dev. 40: 490–502.
White, M. A., A. Ikeda, and B. A. Payseur, 2012a A pronounced evolutionary shift of the pseudoautosomal region boundary in house mice. Mamm. Genome 23: 454–466.
White, M. A., M. Stubbings, B. L. Dumont, and B. A. Payseur, 2012b Genetics and evolution of hybrid male sterility in house mice. Genetics 191: 917–934.
Yang, H., T. A. Bell, G. A. Churchill, and F. Pardo-Manuel de Villena, 2007 On the subspecific origin of the laboratory mouse. Nat. Genet. 39: 1100–1107.
Young, A. C., E. F. Kirkness, and M. Breen, 2008 Tackling the characterization of canine chromosome breakpoints with an integrated in situ/in silico approach: the canine PAR and PAB. Chromosome Res. 16: 1193–1202.

Communicating editor: S. K. Sharan